Innovative Infrastructure Solutions (2025) 10:552
https://doi.org/10.1007/s41062-025-02347-6

TECHNICAL PAPER

Assessing structural resilience of masonry chamber-housed substations subject to flood flow and debris impact

Wenzhu Li[1] · Lee S. Cunningham[1] · David M. Schultz[2] · Sarah Mander[1] · Chin Kim Gan[3] · Mathaios Panteli[4]

Received: 7 March 2025 / Accepted: 5 October 2025

Abstract
Chamber-housed substations are a common substation type, essential for voltage regulation, load balancing, and fault isolation to ensure power supply grid stability and reliability. As typically ground-based structures, chamber-housed substations are vulnerable to damage from flooding. In the case of chambers constructed from plain masonry, these may be susceptible to structural damage from forces generated by flood flows. Although previous studies have examined substation failures based on flood levels, they often overlook the structural damage caused by moving floodwaters and floating debris, thereby underestimating risks and overestimating substation resilience. The present study introduces an analytical framework that uses computational fluid dynamics (CFD) coupled with finite element (FE) analysis to predict flood forces and structural responses in a level of detail that would hitherto not be possible with existing design code approaches. The CFD-based modelling approach was validated against existing hydraulic experiments and subsequently applied to a case study of a typical masonry chamber-housed substation in Malaysia, a country prone to severe annual flooding. The results reveal that substation walls can withstand flood velocities up to 10 m/s without debris. However, the presence of debris leads to damage at velocities below 2 m/s, highlighting a significant reduction in resilience. Fragility and risk curves, derived from a normalised Weibull function, further reveal that ignoring debris impact underestimates forces on walls by 60% to 83%. These findings highlight the need to update design guidelines to account for debris impact and to develop suitable retrofitting strategies for existing chambers.

Keywords Computational fluid dynamics (CFD) · Finite element (FE) · Flooding · Malaysia · Power infrastructure · Structural resilience · Substations

Introduction

Substations are crucial to power systems, managing voltage regulation, load balancing, fault isolation, switching, and protection. These functions ensure efficient power flow control, safeguard equipment, and maintain system reliability and stability. Given their crucial function, the failure of a substation can disrupt an entire power system. Despite their importance, substations are often vulnerable to flooding, as demonstrated by past incidents. Flooding is

✉ Wenzhu Li
wenzhu.li.working@outlook.com

Lee S. Cunningham
lee.scott.cunningham@manchester.ac.uk

David M. Schultz
david.schultz@manchester.ac.uk

Sarah Mander
s.mander@manchester.ac.uk

Chin Kim Gan
ckgan@utem.edu.my

Mathaios Panteli
panteli.mathaios@ucy.ac.cy

[1] Department of Civil Engineering and Management, University of Manchester, Manchester M13 9PL, UK

[2] Centre for Crisis Studies and Mitigation and Department of Earth and Environmental Sciences, University of Manchester, Manchester M13 9PL, UK

[3] Faculty of Electrical Technology and Engineering, Universiti Teknikal Malaysia Melaka, 76100 Melaka, Malaysia

[4] Department of Electrical and Electronic Engineering, University of Cyprus, 20537 Nicosia, Cyprus

Published online: 15 November 2025

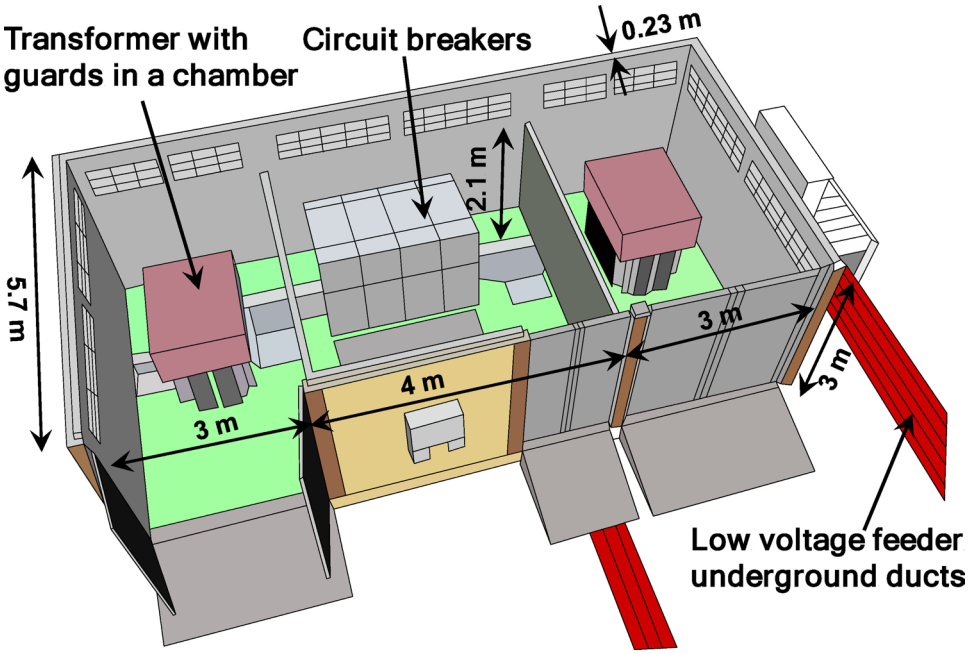

Fig. 1 A typical chamber-housed substation in Malaysia (redrawn from Fig. 4, 5, 6, 7 and 8 in [5]), housing flood-prone equipment such as transformers and circuit breakers, is analysed in the case study presented in Section "case study: flood impact on typical chamber-housed substations"

Fig. 2 Damage to a masonry wall resulting from flash floods in Wenchuan, China, reproduced with permission from [6]

a pressing global issue, and the effects of climate change mean that many parts of the world will experience increased flood frequency and intensity. Presently, many parts of the world are already experiencing frequent severe flooding, one such country being Malaysia. The International Disaster Database (EM-DAT), which compiles data from UN Agencies, non-governmental organisations, the insurance sector and press agencies, has records of 74 of the most severe floods in Malaysia between 1900 and 2024 [1]. The 2014 flood was one of the most devastating, shutting down over 10,000 substations and disrupting power for 200,000 users across urban and rural areas [2]. More recent floods, including those in 2021 and 2023, further highlight the persistent vulnerability of Malaysia's power infrastructure to severe flooding [3, 4].

Chamber-housed substations (e.g., Fig. 1) are typically located at ground level and often constructed from unreinforced masonry [5], which exhibits low tensile strength, limited ductility, and poor energy dissipation capacity [6–8]. These characteristics make unreinforced masonry structures highly susceptible to brittle failure, out-of-plane wall collapse, and rapid crack propagation under dynamic or lateral loads. Consequently, when subjected to hydrostatic pressure, fast-moving floodwaters, or debris impacts (Fig. 2) [9],

such substations are at heightened risk of structural damage, service interruption, and cascading grid failures.

Understanding the failure mechanisms of masonry chamber-housed substations is crucial for developing effective flood resilience measures, yet it remains challenging due to the complex interactions of floodwater and debris. From the limited available studies on substation resilience [10–13], the focus has primarily been on static flood levels and inundation risks. These studies assessed failure probabilities and recovery times based only on flood depth, recommending defences such as demountable dams [10] and equipment elevation [11]. However, existing studies have largely overlooked the effects of hydrodynamic forces and floating debris, which may underestimate actual risks and overestimate flood resilience. This issue is highlighted by Li et al. [14], which emphasises the need to incorporate these factors into flood resilience assessments to achieve more accurate and comprehensive risk evaluations. Whereas direct studies on structural failure of chamber-housed substations under flood conditions are limited, complementary research on similarly constructed buildings, such as masonry residential structures, provides valuable insights. For example, Si et al. [9] established brittle failure criteria for rural buildings with single-span masonry walls, which share structural similarities with masonry-built chamber-housed substations. Furthermore, Jansen et al. [15] examined the effects of hydrodynamic forces on masonry walls, using experimental and modelling approaches to develop fragility curves. These findings help understand substation chamber behaviour under flood conditions and serve as a basis for defining structural failure thresholds and probabilities for chamber-housed substations in the present study.

Nevertheless, although the effect of flood flow was considered by Si et al. [9] and Jansen et al. [15], they neglected the critical role of debris in the fluid and structure interactions. As a result, current research still falls short of fully addressing the flood resilience of chamber-housed substations. Therefore, the present study addresses these gaps by:

1. Incorporating hydrodynamic and debris impacts to more accurately model flood risks.
2. Employing advanced computational fluid dynamics (CFD) and finite element (FE) coupling for precise simulation of structural behaviours under flood conditions.
3. Developing fragility and risk curves, and quantifying failure probabilities specific to substations.

Various approaches can be considered to account for the impacts of hydrostatic, hydrodynamic, and debris on chamber walls. Experimental testing can provide valuable physical data on complex hydrodynamic forces and structural responses; however, such tests are often constrained by high costs and practical limitations [16]. Alternatively, simpler analytical methods, such as FEMA P-55 [17], are by necessity simplified and may not capture the intricate interactions between hydrodynamic forces and structural behaviour. Given these challenges, CFD models coupled with FE analysis emerge as a more practical and effective approach, enabling detailed simulations of the relevant forces and structural responses while overcoming the limitations of experimental and analytical methods.

Based on the above, the present study employs 3D CFD modelling using the Reynolds-Averaged Navier–Stokes (RANS) approach, coupled with a finite element (FE) model to implement one-way interaction between the fluid and the structure. In the adopted CFD approach, the fluid exerts forces on the structure, but the structure does not deform or influence the fluid flow in return. This simplification is considered appropriate for the relatively rigid structural forms examined in this study, i.e. where the masonry walls are comparatively thick and there are closely spaced return walls providing significant lateral stiffness. Previous research has demonstrated the suitability of this approach in capturing fluid–structure interaction with a good level of accuracy. For instance, Elrond [18] demonstrated how 3D CFD modelling could simulate interactions between floodwaters and building structures, highlighting increased impact forces near inflow points. Ahmadi et al. [19] employed a RANS-based model combined with the k-ω turbulence model to simulate supercritical flows, calculating hydrodynamic pressures and water levels on cylindrical and rectangular bridge piers during floods. Zhang and Wang [20] applied a one-way fluid–structure interaction method to model the stress distribution in bridge structures under flood conditions. Such works collectively offer methodological insights for the present study's use of CFD modelling to simulate the effects of flooding on substation chamber structures.

The remainder of this paper is structured as follows. Firstly, the proposed CFD-based modelling approach is validated by simulating existing experiments, demonstrating its accuracy in accurately capturing the key hydrodynamic behaviour (Section "Validation of the computational fluid dynamics (CFD) model"). Then, threshold, fragility and risk curves, derived from the numerical modelling results, are developed to illustrate the respective failure conditions and probabilities for chamber-housed substations (Sections "Case study: flood impact on typical chamber-housed substations" and "Structural resilience analysis for substation chambers"). Finally, the present study concludes with strategies for using these curves to enhance the resilience of masonry-built chamber-housed substations (Section "Conclusion").

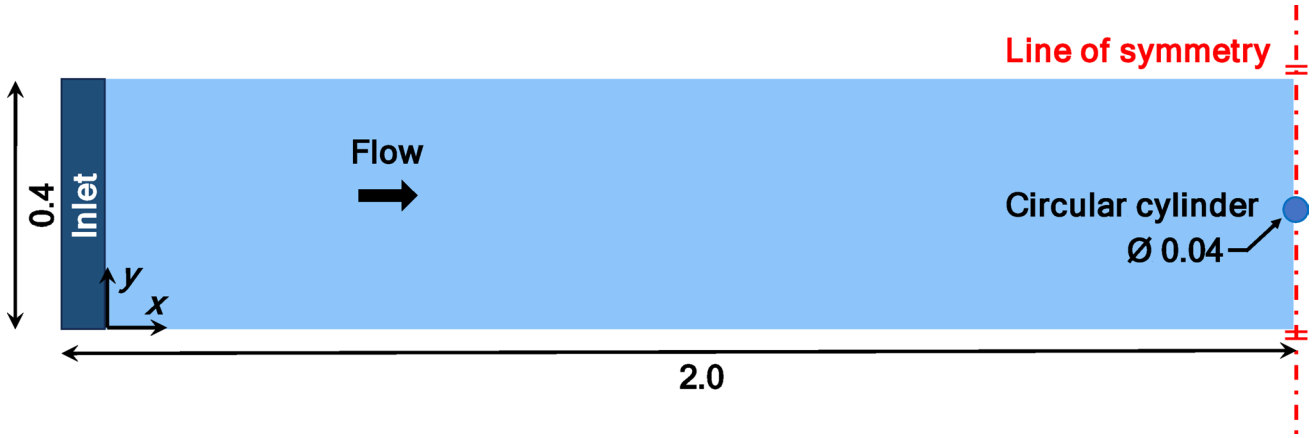

Fig. 3 Validation 1: Plan view of flume layout with circular cylinder and flow direction (all dimensions in meters)

Table 1 Mesh strategies M1 to M5 for sensitivity analysis in CFD simulations

Dimension	Size (mm)	Number of elements in each dimension				
		M1	M2	M3	M4	M5
Depth	60	2	4	8	12	16
Width	400	4	8	16	24	32
Length	4,000	8	16	32	48	64

Validation of the computational fluid dynamics (CFD) model

To ensure reliability, the proposed CFD-based modelling approach, validated against two experiments (one for hydrodynamics without debris and another incorporating floating debris), uses ANSYS Fluent 2022R1 for its robust handling of fluid–structure interactions [21]. The simulations solve the RANS equations for incompressible flow, including the continuity equation ($\partial_{ut}/\partial_{xi}=0$) and momentum equation [22], with turbulent stresses modelled using the Shear Stress Transport (SST) k–ω turbulence model [23]. This model is chosen for its ability to accurately capture near-wall and free-stream turbulence effects. A mesh sensitivity analysis determines optimal grid resolution, balancing accuracy and computational efficiency. Key constants, such as water density (1000 kg/m^3) and dynamic viscosity (1.002×10^{-3} Pa s), are incorporated [24], with boundary conditions and solver settings designed for transient simulations. This approach provides a reliable and practical method for analysing flood-induced forces and structural responses in substation chambers.

Validation 1: hydrodynamic flow around an object

In Validation 1, the experimental study by Ducrocq et al. [25] was selected as it provides high-quality data on the interaction between floodwaters and a solid structure, in this case, a free-surface-piercing cylinder. Moreover, the study covers a wide range of flow conditions and includes measurements of drag forces and water surface elevations, which are suitable for validating both flow patterns and surface profiles in the present numerical model.

In the selected experiment, a cylinder of 0.04 m diameter was fixed to the bed at the centreline of a flume, which measured 0.4 m in width and 4 m in length (Fig. 3). By representing the original experimental setup, the CFD simulation was conducted at a flow rate of 10 l/s and an upstream water depth of 0.06 m over a flatbed slope. The renormalisation group SST k–ω turbulence model was employed to capture near-wall effects, with the simulation running for 15 s to reach a steady flow state. The flow zone and the cylinder were meshed with hexahedral elements, chosen for their geometric simplicity and ability to ensure good convergence with fewer elements and reduced computational time.

Following the initial setup of the experimental conditions in the flume, a mesh sensitivity analysis was conducted to ensure the accuracy and stability of the CFD model. This analysis employed five different meshing strategies, labelled M1 to M5 as detailed in Table 1, each varying the number of elements across the tank's dimensions: height (60 mm), width (400 mm), and length (4,000 mm).

The meshing strategies in Table 1 apply specifically to the upstream zone, whereas the mesh will become finer as it approaches the object. Such a strategic mesh refinement technique is illustrated in Fig. 4, where mesh density is increased near the central column to accommodate the transition from rectangular to circular geometries.

Additionally, the top right zoomed-in view of Fig. 4 shows how the mesh smoothly transitions from a square to

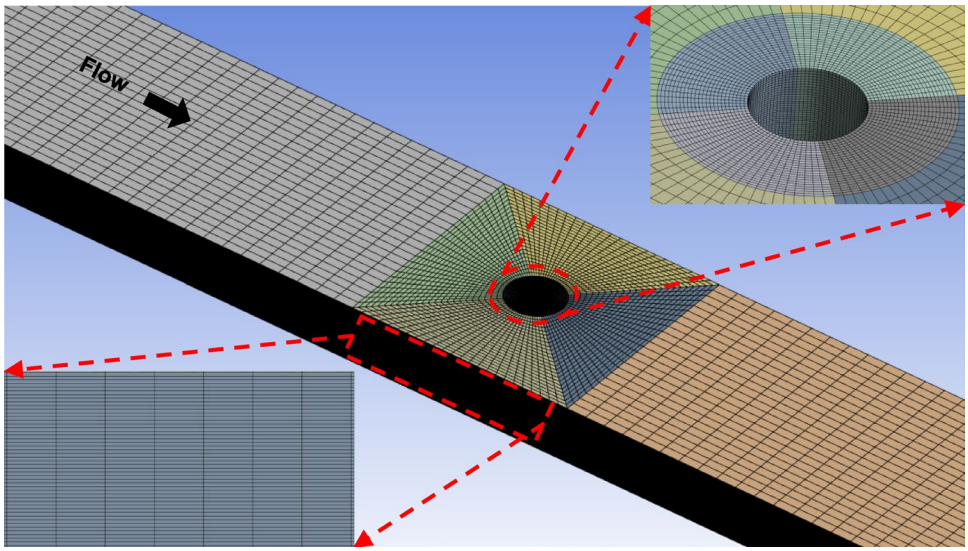

Fig. 4 Mesh configuration for Validation 1, featuring gradual refinement near the cylindrical structure

Table 2 Mesh strategies M1 to M5 for sensitivity analysis in CFD simulations

Mesh ID	CFD		Experimental Drag coefficient	Error in CFD compared to experiment (%)
	Drag force at 10 s (N)	Drag coefficient		
M1	0.87	4.18	1.20 to 1.79, the average value is 1.50	179.60
M2	0.42	2.00		33.78
M3	0.34	1.64		9.70
M4	0.34	1.65		10.37
M5	0.34	1.61		7.69

a circular pattern, optimising uniformity in less complex areas. Meanwhile, the bottom left view displays a consistent rectangular mesh through depth. Different mesh colours represent levels of refinement: grey for regular fluid flow areas; green and yellow for areas with complex dynamics such as bends; and blue and orange for regions with higher flow velocities or pressure variations. Such refinement improves computational accuracy and convergence, essential for accurately simulating fluid dynamics during fluid–structure interactions.

During the CFD simulations in ANSYS Fluent, the drag force F_{drag} at any time (e.g., at 10 s when floodwater bypassed the cylinder) can be obtained on the cylinder (treated as a rigid body). The drag coefficients C_d, crucial for evaluating fluid dynamics around obstacles, were then derived using Eq. (1). Table 2 shows that the drag coefficients stabilised between mesh sizes M3 to M5, with a ~ 10% error margin compared to experimental values ranging from 1.20 to 1.79 [25], under the same flow, depth, and cylinder conditions.

$$C_d = \frac{2F_{drag}}{\rho d D {v_f}^2}, \tag{1}$$

where ρ and d = density and depth of the flow, respectively; D = diameter of the cylinder; and v_f = flow velocity.

Furthermore, Fig. 5 explores the CFD model's accuracy by showcasing the free surface elevation around the cylinder, which is another critical metric for assessing hydrodynamic behaviour. As the mesh was refined from M1 to M5, water level predictions on both upstream and downstream sides aligned better with the experimental data. Upstream (negative x/D), the water is undisturbed by the cylinder, so changes in mesh density (from M1 to M5) have minimal effect on water surface elevation. However, downstream, the flow is significantly influenced by the cylinder, making the simulation results more sensitive to mesh refinement. Therefore, finer meshes provide improved agreement with experimental data, especially for downstream. Among them, meshes M4 and M5 deviated by just 10% from experimental observations in [25], demonstrating relatively accurate simulation of turbulent flows around obstacles.

Given the balance between computational efficiency and accuracy, the M4 mesh strategy was selected for the subsequent case study. This choice is also supported by stabilising drag coefficients between mesh M3 and M5.

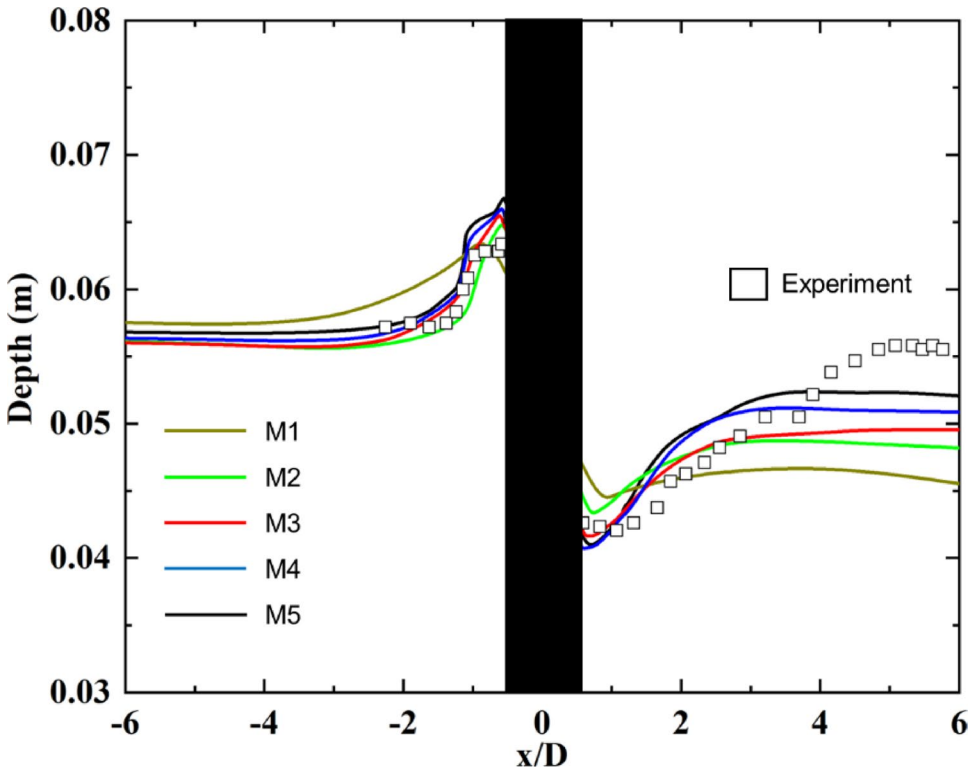

Fig. 5 Validation 1: Comparison of numerical and experimental water surface elevation along the flume centreline (x = streamwise distance along flume from cylinder, D = cylinder diameter)

Table 3 Impact force comparison for various debris (0°: debris length parallel to the wall)—left columns: experimental setup, right columns: results

Flow velocity (m/s)	Debris size (cm)	Debris mass (kg)	Impact angle (°)	Numerical force (N)	Experiment force (N)	Error (%)
0.381	8.9 × 14 × 91	5.90	0	655	589	11.27
0.533	14 × 14 × 91	12.00	0	1768	1466	20.59
0.800	19 × 19 × 91	14.40	90	2430	2311	5.18
0.800	19 × 19 × 91	19.70	90	3754	3032	23.80

Validation 2: floating debris impact

Next, to validate the model's ability to simulate the impact of floating debris, the experimental work by [26] was selected. This experiment analysed the dynamics of scaled idealised logs impacting a wall, considering flow velocity (as a scalar magnitude without direction), log mass, and impact direction. Four test series, closely representing field conditions, were chosen for this validation (Table 3).

The proposed CFD model replicates the experimental setup (Fig. 6) but reduces the simulated flume length to 7.6 m for computational efficiency, following the method in [27]. The meshing density, measured as elements per square meter, is consistent with previous validation studies (M4). Both the log debris and the impacted wall were modelled with Young's modulus of 5 GPa as per the experiment. The timber log was represented using hexahedral elements, with three elements through its thickness. Due to the high relative stiffness of the objects, resulting in minimal deformation and negligible impact on the hydrodynamics, one-way coupling was chosen to balance accuracy and efficiency. This approach was also used in the subsequent case studies in section "case study: flood impact on typical chamber-housed substations". The CFD simulation utilised two modules in ANSYS Fluent: the FLUENT module, which assigned the same initial velocity to the water and floating log to capture debris velocity and pressure history against the wall, and the MECHANICAL module, which then simulated the wall's structural response based on these pressure time-histories.

In a previous numerical study by [27], a coupled Eulerian–Lagrangian approach was used, but the simulations deviated from experimental results by 54.3%. In contrast, this work uses the SST k–ω turbulence model and a Six Degrees of Freedom (Six DOF) model to accurately simulate debris movement and impact in 3D space [28], achieving an improved level of accuracy.

To be specific, as shown in Table 3 and Fig. 7, the absolute error between simulation and experimental impact force ranges from 5.18% (at 0.8 m/s with a 14.4 kg debris at 90°) to 23.80% (at the same velocity but with a heavier 19.7 kg debris). To quantify the overall agreement, the overall Root

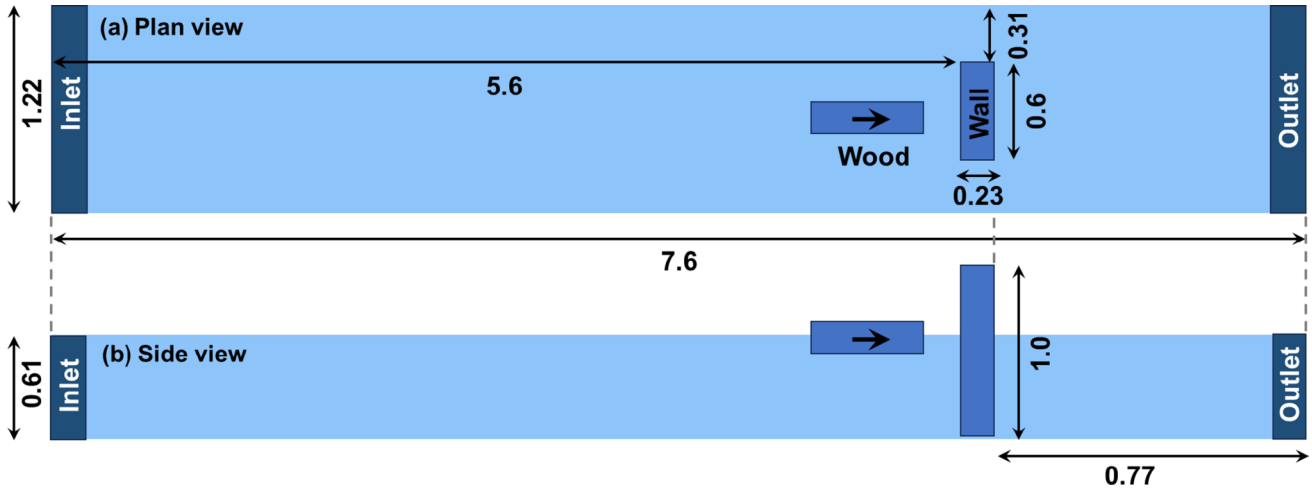

Fig. 6 Validation 2 for debris impact: plan view (top) and side view (bottom) of the numerical domain

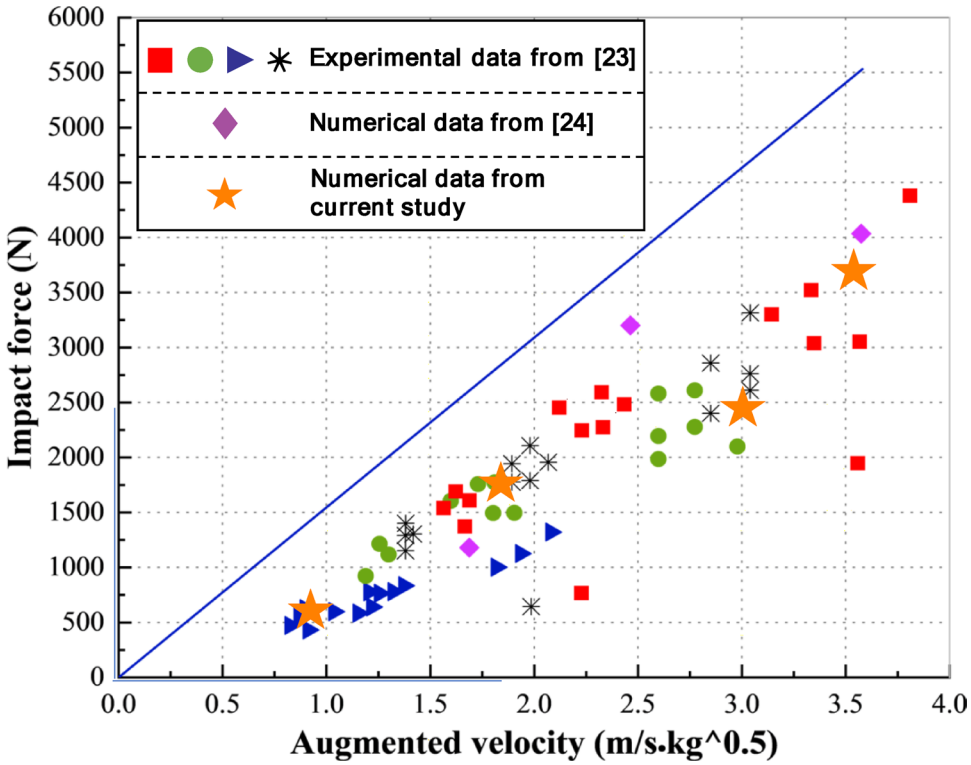

Fig. 7 Comparison of CFD results from the present study with corresponding results from experiments by [23] and numerical modelling by [24]

Mean Square Error (RMSE) is calculated as 397.18 N, and the Coefficient of Variation (CoV) is 21.47%, indicating a reasonable level of agreement with experimental data.

$$\mathrm{RMSE} = \sqrt{\frac{1}{n}\sum_{i=1}^{n}\left(F_i^{\mathrm{CFD}} - F_i^{\mathrm{EXP}}\right)^2} = 397.18\ \mathrm{N} \tag{2}$$

$$\mathrm{CoV} = \frac{\mathrm{RMSE}}{F^{\mathrm{EXP}}} \times 100\% = 21.47\% \tag{3}$$

Nevertheless, larger discrepancies at higher velocities are attributed to intensified turbulence, wake flow, and complex fluid–structure interactions not fully captured in the numerical model. In addition, impact angle variation in the experiment may introduce further uncertainty.

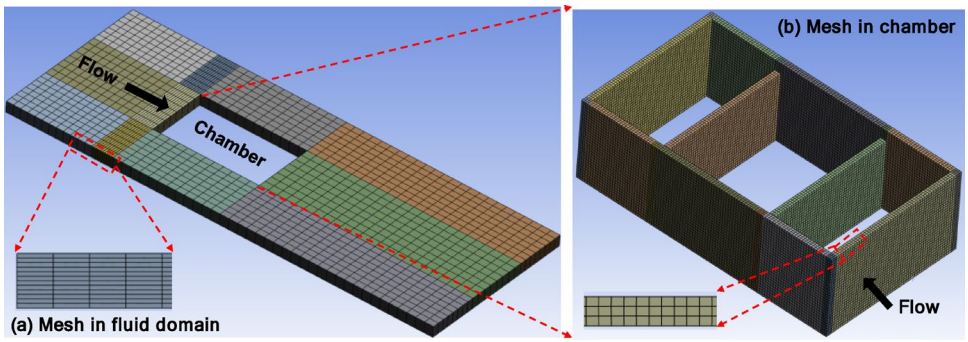

Fig. 8 Mesh diagram in (**a**) flume domain and (**b**) substation chamber

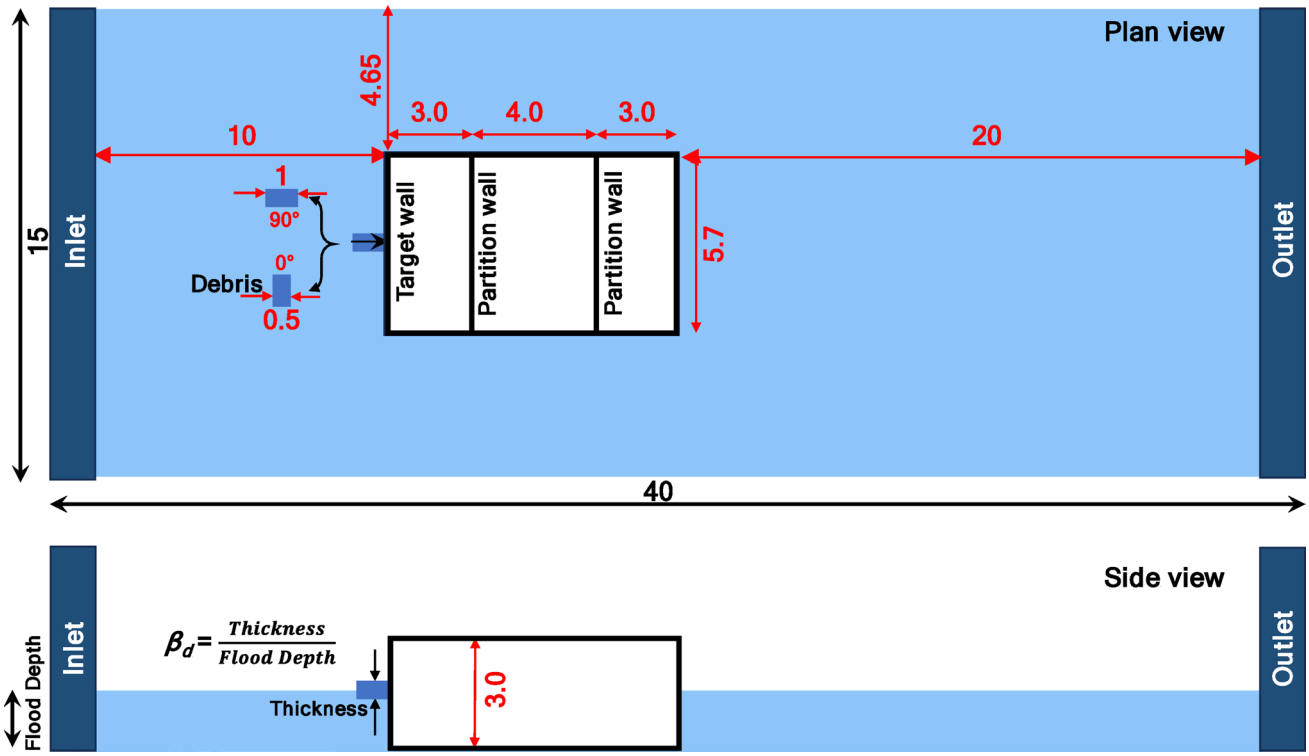

Fig. 9 Schematic diagram of the numerical flume and substation chamber

Case study: flood impact on typical chamber-housed substations

The previous section validated the CFD-MECHANICAL modelling approach for simulating hydrodynamic and floating debris effects. This section presents a case study of a typical masonry chamber-housed substation, commonly found in Malaysia (Fig. 1). The Malaysian design is chosen here since the country has an abundance of masonry substations and experiences regular flood events.

Currently, in Malaysia, masonry chambers are designed according to the European standard Eurocode 6 [29]. Hence, this form of construction is not confined to Malaysia and can be found elsewhere in the world. The meshing strategy from Validation 1 (M4) is applied to the fluid domain, with similar mesh refinement close to the object. Meanwhile, the meshing strategy for the structure from Validation 2, which uses three solid elements through the wall thickness, is employed for the masonry walls (Fig. 8). The masonry is treated as a continuum using the macro modelling approach similar to [30]. The structural model in this study is elastic, with the Young's modulus of the masonry system set at 5 GPa, as per [30].

This study assumes that debris, as shown in Fig. 9, travels at the same velocity as the surrounding flood flow, and is set as rectangular for two main reasons:

(a) Experimental consistency: The referenced experimental study [25] used rectangular wooden planks as debris.
(b) Modelling consistency: Previous numerical studies (e.g., [27]) also adopted rectangular debris, and our model follows the same assumption to ensure comparability.

Besides, in this study, tensile failure was expected to be the governing criterion, defined as the point at which the tensile stress reaches the strength of the fired clay brickwork masonry. As tensile failure is primarily influenced by debris mass and velocity, these factors have been considered in the model. The debris cross-sectional shape can affect the localised pressure on the wall; a broader parametric study incorporating different debris geometries will be explored in future work.

The case study models the entire substation chamber (dimensions detailed in Fig. 9) and focuses on the masonry wall with the largest horizontal span between return walls, termed the 'target wall' (3 m height, 5.7 m width, 0.23 m thickness), as it experiences the highest bending moments and shear forces (structural response). The substation chamber is assumed to be watertight. Namely, the flood levels are below that of the air vents positioned at the top of the building (Fig. 1). All the substation walls are 0.23 m thick and constructed from fired clay bricks bonded with a 1:3 cement–sand mortar. The masonry flexural and shear strengths (structural capacity) are determined using the approach outlined in Eurocode 6. By applying the criterion 'structural response = structural capacity,' the failure threshold can be evaluated.

Setup and simulations of flood scenarios

To balance time and efficiency, this study simulates 84 typical flood scenarios by varying key parameters: water velocity and depth, debris size and its impact angle (illustrated in Fig. 9). The scenarios cover both the case of no-debris and with-debris.

For the with-debris cases, rectangular plank wooden debris, consistent with Validation 2, is used. The debris scenarios include two impact angles, four flood depths, and three variations in flood velocity and debris size. The specific values were selected based on the following rationale:

(a) Angles of 0°/90° refer to the debris's longest side being parallel or perpendicular to the wall, respectively, with the impact always centred. The debris starting point is set by flood velocity (e.g., 0.5 m/s velocity means a 0.5 m initial distance) to ensure the impact occurs within 1 s for computational efficiency.
(b) Flood depths (0.25, 0.5, 1.0, and 1.5 m) were based on practical considerations and field observations, for example, in [31].
(c) Debris sizes were scaled relative to flood depths as indicated by the factor β_d (debris thickness/flood depth shown in Fig. 9), with $\beta_d = 0$ (no debris) and $\beta_d = 0.2$, 0.4, and 0.6, ensuring realistic proportions, as smaller or larger sizes showed less impact or diminishing returns in failure rates [14].
(d) Velocities were scaled to represent a range from slow to fast based on observed flood velocities in the field [32].

Structural response of substation wall to flood flow

This section analyses 84 simulation results to understand the impact process and structural response to floodwater and debris, intending to evaluate potential structural failure in substation chambers. Using flood depth = 1.0 m, flood velocity = 0.25 m/s, $\beta_d = 0.4$ as an example, the structural response is represented by stress distributions within the target wall at various stages (e.g., points A, B and C in Figs. 10 and 11).

Figures 10 and 11 show that before the debris impact (e.g., at $t = 0.05$ s and $t = 0.15$ s), the chamber wall was subjected to stress from hydrostatic and hydrodynamic forces. During this period, the upstream face of the wall at the waterline was under compression, whereas the corresponding downstream face experienced tensile stress. The time-history curves reveal that the maximum stresses are around 0.05 MPa, which is well below the Eurocode's specified range of characteristic strengths for clay-fired brick masonry walls (flexural strength: 0.25–0.7 MPa; shear strength: 0.1–0.3 MPa [29]).

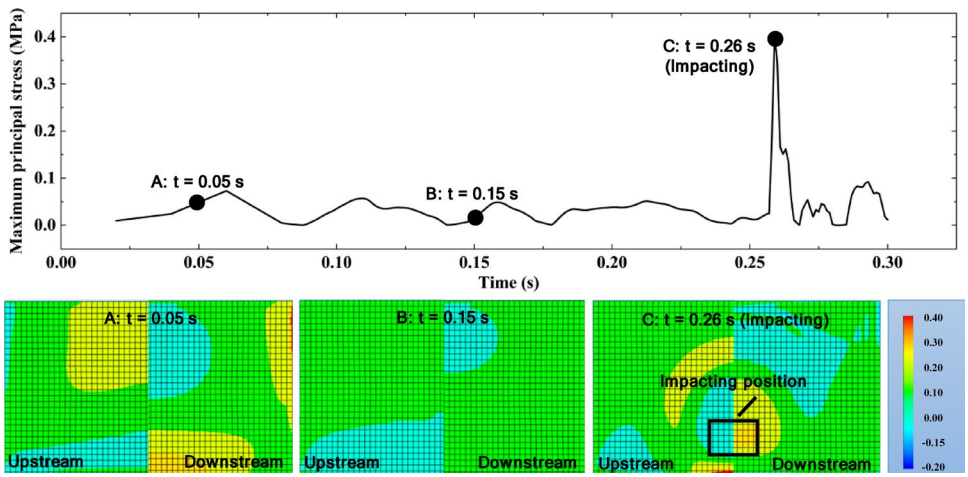

Fig. 10 Time history and contour plot of maximum principal stress (MPa) in the target wall during the debris impact process (the symmetrical half is shown)

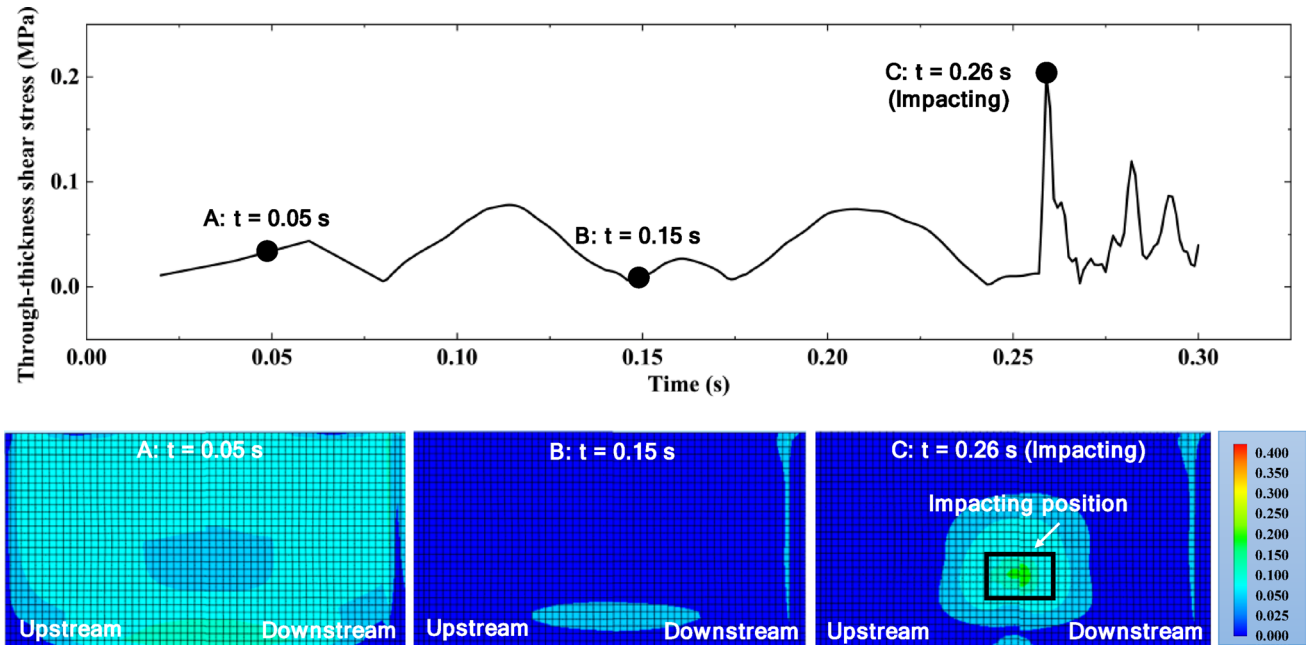

Fig. 11 Time history and contour plot of maximum through-thickness shear stresses (MPa) in the target wall during the debris impact process

However, when the debris impact occurred (t=0.26 s), the maximum principal stress and through-thickness shear stress surged to around 0.4 MPa and 0.2 MPa, respectively. The stresses before impact represented only 17.5% and 40% of the maximum principal and shear stresses at the moment of impact. These findings highlight the significant role of debris impact as a primary factor in structural failures of substation walls, emphasising that it cannot be overlooked.

Threshold curve development for failure evaluation

To identify the hydraulic and debris scenarios that could lead to the failure of the substation wall, this section develops threshold curves by interpolating between simulated data sets. The velocity range was selected to ensure that the resulting stress values span a range that includes the characteristic flexural and shear strengths of the wall. The following steps outline the process for developing these threshold curves.

Step 1: Determination of the interpolation function

As previously mentioned, the characteristic flexural strength of fired clay brickwork masonry (with failure planes parallel to bed joints, i.e., the weakest orientation) generally ranges between 0.25 and 0.7 MPa [29]. For calculation purposes, a representative value of 0.5 MPa was adopted (i.e., for masonry with M12 mortar and clay fired brick units with a water absorption rate between 7 and 12%). The focus of this study is on developing a scalable fragility-based assessment framework. Users may opt for more conservative values, such as the lower bound of 0.25 MPa, based on specific design needs or risk preferences. In this case, the mid-range value of 0.5 MPa was deemed sufficient to demonstrate the method's applicability.

Then, at any given flood depth, the linear interpolation function (f) can be determined using Eq. (4) based on the simulated maximum flexural stress (σ_{over} or σ_{below}).

$$f = \frac{\sigma_{\text{over}} - 0.5}{\sigma_{\text{over}} - \sigma_{\text{below}}}, \tag{4}$$

where σ_{over} is the simulated maximum flexural stress just over 0.5 MPa, and σ_{below} is just below 0.5 MPa.

Figures 12 and 13 show results from 84 simulations, with velocity as input and resulting stress as output. For example, from Fig. 12b, at a flood depth of 0.5 m with no debris, the maximal flexural stresses are 0.17 MPa at a flood velocity of 5 m/s (Point A); 0.55 MPa at 10 m/s (Point B); and 1.67 MPa at 15 m/s (Point C). In this case, σ_{over} is 0.55 MPa and σ_{below} is 0.17 MPa, so that f is calculated as 0.87. This interpolation value indicates that the flexural stress of 0.5 MPa is reached at a flood velocity between 5 and 10 m/s.

Step 2: Determination of flood condition triggering structural failure (i.e., threshold velocity accounting for a specific flood depth)

In the example mentioned, the velocity when the flexural stress reaches 0.5 MPa is the threshold velocity ($v_{\text{threshold}}$). To determine it, the linear function (f) is used to interpolate between two velocity points corresponding to the stresses σ_{over} and σ_{below}.

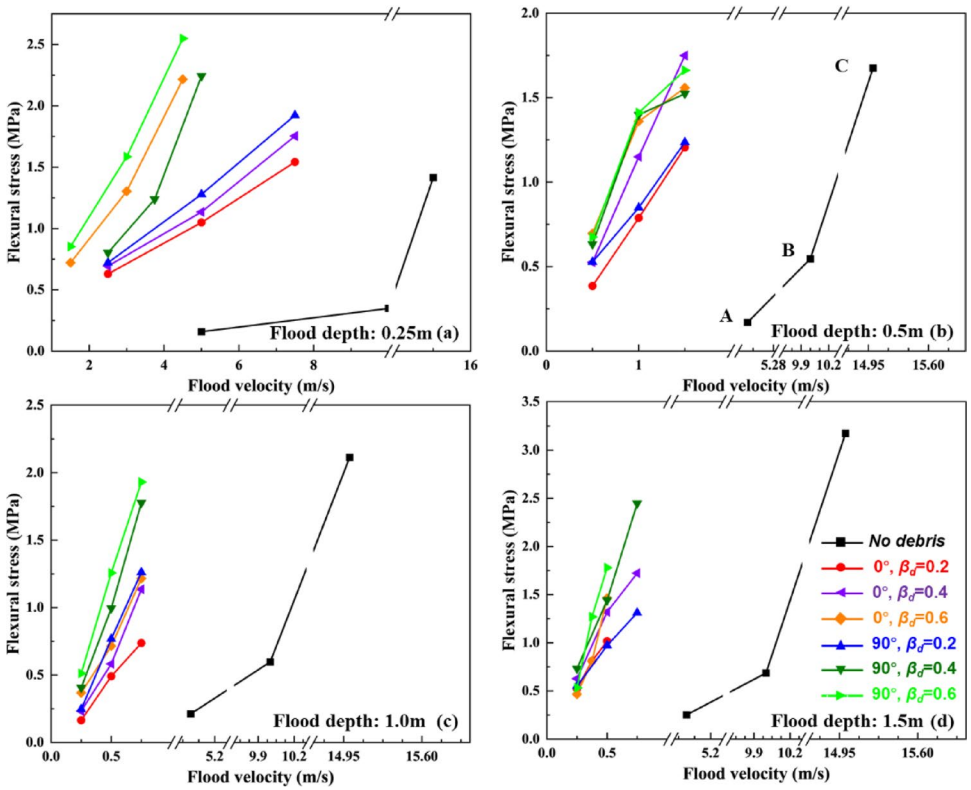

Fig. 12 Peak flexural stress in masonry vs. corresponding flood velocity for various flood depths

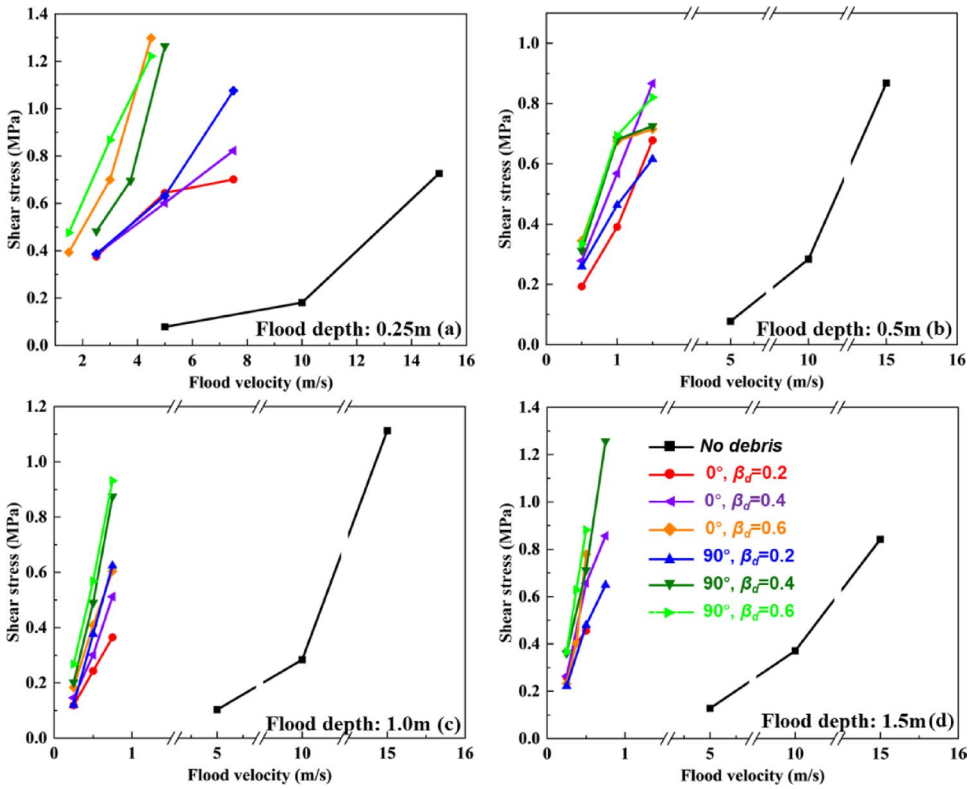

Fig. 13 Peak shear stress in masonry vs. corresponding flood velocity for various flood depths

$$v_{\text{threshold}} = f \times (v_{\text{over}} - v_{\text{below}}) + v_{\text{below}}, \quad (5)$$

where v_{over} is the input flood velocity corresponding to the simulated maximal flexural stress just over the 0.5 MPa; v_{below} is the input flood velocity corresponding to flexural stress just below 0.5 MPa.

The same steps can be conducted to find the threshold velocity for shear stress. 0.3 MPa is used as the characteristic shear strength of fired clay brickwork masonry, which generally ranges between 0.1 and 0.3 MPa (failure plane parallel to bed joints) [29].

As a result, Fig. 14 presents the threshold curves that illustrate the flood conditions capable of triggering structural failures in the substation chamber. As previously stated, these curves are based on simulated scenarios, considering debris impact angles of 0° and 90°, debris size factors (β_d) of 0.2, 0.4, and 0.6, as well as scenarios with no debris. Eurocode 6 includes a material safety factor (γ_M) by which the characteristic strength values are reduced to produce a design stress. The value of γ_M depends on the quality and consistency of material manufacturing and construction control. In the current study, this is set at 2.3, representing standard manufacture and construction control [33], and 1.0 for comparison, representing no material factor. The impact of material safety factors on the threshold curves is illustrated in Fig. 14.

Debris significantly lowers the failure thresholds, thus increasing structural failure risk. For instance, Fig. 14a shows that without debris, the threshold flood velocity for substation failure is 8 m/s. However, with debris, this threshold drops dramatically to below 0.5 m/s, indicating that debris plays a crucial role in structural failure, even in shallow water. As flood depth reaches 1 m, the threshold velocity stabilises. Additionally, when debris impacts

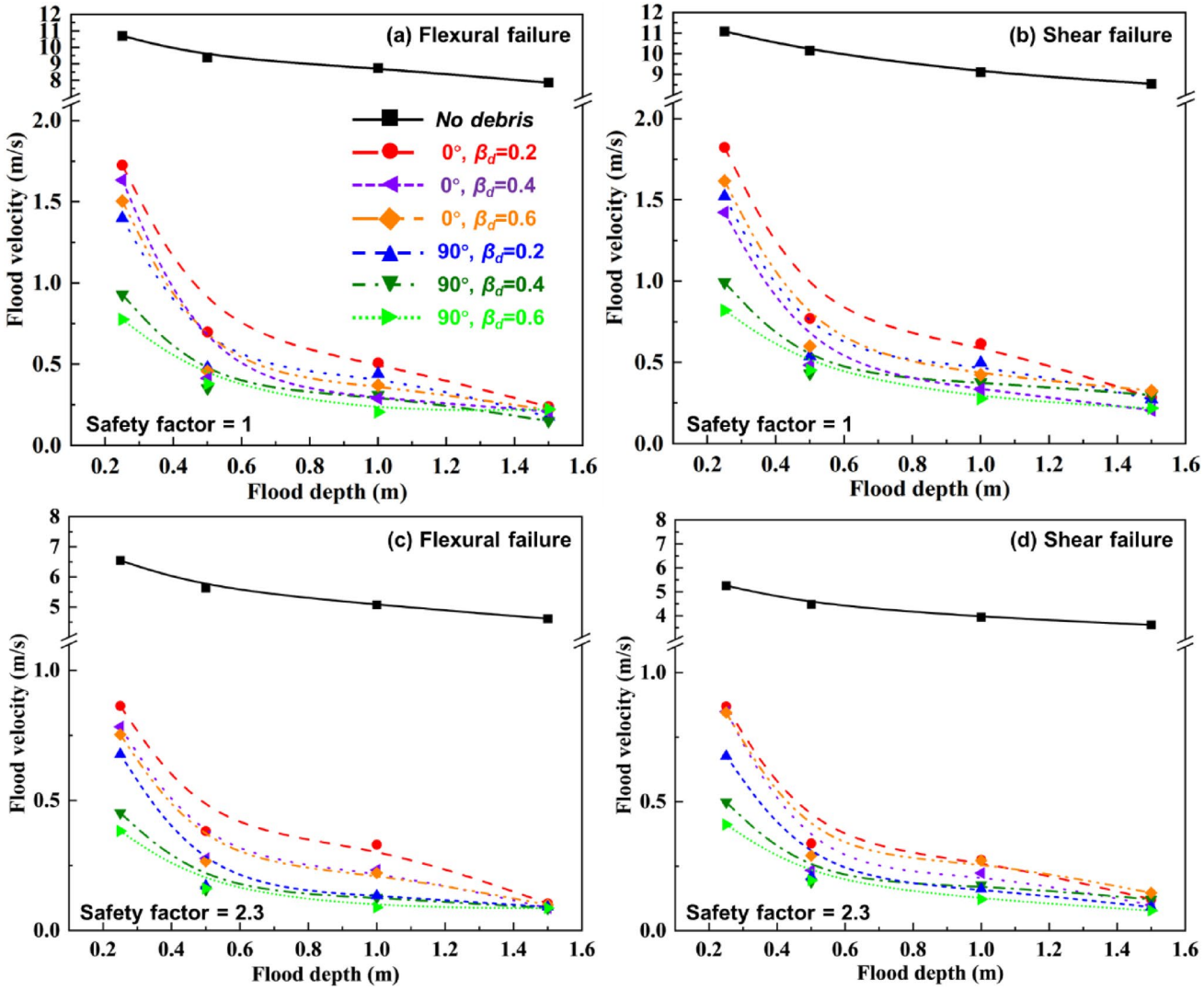

Fig. 14 Threshold curves predicted by the linear interpolation function: with γ_M=1, **a** flexural failure and **b** shear failure; with γ_M=2.3, **c** flexural failure and **d** shear failure

at a 90° angle, the failure threshold is lower due to higher local stresses. The dominant failure mode, whether flexural or shear, depends on their relative capacities. Simulation results (Figs. 12 and 13) indicate that under the same flood conditions, flexural stress is typically twice that of shear stress. Therefore, if the flexural capacity is less than twice the shear capacity, flexural failure will occur earlier, and vice versa.

Moreover, when γ_M increases from 1.0 to 2.3, the threshold curves shift downward regardless of the flow conditions. For example, from Fig. 14a to c, the threshold velocity decreased from 9–11 m/s to 5–7 m/s in no-debris scenarios. Therefore, the material safety factor significantly affects the threshold flood velocity, so a conservative value is recommended for a more resilient substation design.

Structural resilience analysis for substation chambers

The threshold curves indicate the conditions (i.e., any combination of flood depth and velocity) that trigger structural failures in substation chambers. To understand the likelihood of these threshold conditions, the distribution functions for flood depths and velocities need to be determined first. According to a previous study by the authors [14], the normalised Weibull function can be used to describe these distributions, as described in Eqs. (6)–(9).

$$f(h_f;\lambda_h,k)=\frac{\frac{k}{\lambda_h}\cdot\left(\frac{h_f}{\lambda_h}\right)^{k-1}\cdot e^{-\left(\frac{h_f}{\lambda_h}\right)^{k}}}{\frac{k}{\lambda_h}\cdot\left[\left(\frac{k-1}{k}\right)^{\frac{1}{k}}\right]^{k-1}\cdot e^{-\left[\left(\frac{k-1}{k}\right)^{\frac{1}{k}}\right]^{k}}}\quad h_f\geq 0. \tag{6}$$

Equation (6) gives the flood depth distribution, where h_f denotes any flood depth; λ_h is the only unknown parameter and can be obtained by Eq. (7), where h_m is the mode of the depth distribution.

$$\lambda_h=\frac{h_m}{\left(\frac{k-1}{k}\right)^{\frac{1}{k}}} \tag{7}$$

Similarly, the normalised Weibull function to describe the flood velocity distribution is given in Eq. (8).

$$f(v_f;\lambda_h,k)=\frac{\frac{k}{\lambda_v}\cdot\left(\frac{v_f}{\lambda_v}\right)^{k-1}\cdot e^{-\left(\frac{v_f}{\lambda_v}\right)^{k}}}{\frac{k}{\lambda_v}\cdot\left[\left(\frac{k-1}{k}\right)^{\frac{1}{k}}\right]^{k-1}\cdot e^{-\left(\frac{v_f}{\lambda_v}\right)^{k}}}\quad v_f\geq 0, \tag{8}$$

where v_f denotes any flood velocity, and λ_v is the only unknown parameter and can be obtained by Eq. (9). v_m is the mode of the velocity distribution.

$$\lambda_v=\frac{h_v}{\left(\frac{k-1}{k}\right)^{\frac{1}{k}}} \tag{9}$$

These flood depth and velocity distributions can be used to obtain the substation chamber's failure probability by deriving fragility curves (showing failure probability at different flood depths), and risk curves (showing failure probability at different flood return periods). The development of fragility curves is introduced as follows.

Fragility curve development for resilience assessment

To develop fragility curves, the probability of structural failure at any given flood depth must be calculated. The steps are: (1) setting a given flood depth, such as 0.5 m, the threshold flood velocity can be determined regarding a specific threshold curve in Fig. 14; (2) the probability of a substation structure failing at any potential flood depth is the percentage of the tail area enclosed by the curve beyond the threshold flood depth in the flood-capacity threshold curve (Fig. 15). Therefore, the integral formulations are a conditional probability; the horizontal axis represents the flood depth (h_f), as described in Eq. (10) [14],

$$P_h=(v_f\geq v_{f.th}|h_f)=\frac{\int_{v_{f,th}}^{+\infty}f\left(v_f\right)dv_f}{\int_{0}^{+\infty}f\left(v_f\right)dv_f}, \tag{10}$$

where h_f is flood depth, v_f is flood velocity. $v_{f.th}$ is the corresponding threshold flood velocity at a given flood depth, $f(v_f)$ refers to the Weibull probability functions regarding flood velocity.

Based on Eq. (10), Fig. 15 shows fragility curves for chamber-housed substations under six example scenarios, considering different debris sizes and impact angles. Since hydrostatic water pressure and hydrodynamic forces alone are unlikely to cause substation failure, as aforementioned in Section "Threshold curve development for failure evaluation", the failure probability for scenarios without debris is relatively low and, therefore, not provided. For demonstration, λ_v in the Weibull function is assumed to be 0.85, which has been validated in [14].

From Fig. 15, structural failure under shallow water conditions (≤0.5 m) is highly sensitive to the size and impact angle of debris. For instance, increasing debris size β_d from 0.2 to 0.4 doubled the failure probability based on maximum flexural stress, and increased it by 50% based on shear stress. Changing the impact angle from 0° to 90° raised failure probabilities by 50–125% and 25–40%, respectively. In such scenarios, mitigation strategies should focus on preventing direct debris impact. This can be achieved by

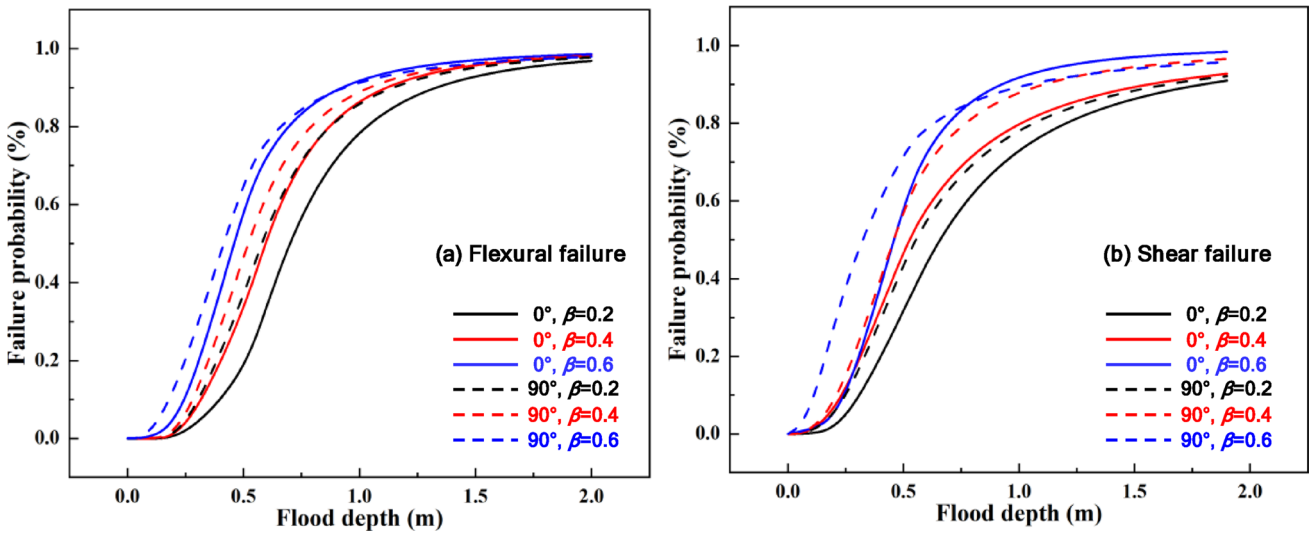

Fig. 15 Fragility curves for substation chambers at increasing flood depth when γ_M=1: **a** flexural failure; **b** shear failure

installing debris deflection systems upstream of substations, applying protective shielding to vulnerable wall sections using materials such as steel mesh or reinforced panels, and reinforcing local wall areas where impact is most likely to occur. These targeted interventions can help reduce structural vulnerability under low-depth but high-variability debris conditions.

As the flood depth increased to 1.5 m, the failure probabilities under different debris conditions began to converge, reaching nearly 100%, where hydrodynamic forces dominate and debris effects become less distinguishable, design priorities shift toward holistic protection measures. These include global structural strengthening of the substation walls, elevation of critical electrical equipment to avoid direct water contact, and adjusting site location or platform height to prevent severe inundation. Such depth-specific mitigation strategies can support resilience-based upgrades and the development of new substations in flood-prone regions, ensuring a balanced consideration of risk, cost, and functional continuity. Therefore, in practical terms, a 1.5 m flood depth should be considered a critical threshold at which the substation is at high risk of failure.

Risk curve development for resilience assessment

Risk curves complement fragility curves in assessing the failure probability of the masonry chamber-housed substations. The horizontal axis of the risk curve represents the flood return period (T), whereas the vertical axis shows the exceedance probability.

In Step 1, representative flood return periods of 2, 5, 10, 15, and 20 years are selected as inputs. Step 2 then fits a normalized Weibull distribution to flood depths, from which the exceedance probability for each return period is obtained. For instance, a 5-year return period (T=5) yields an exceedance probability of 0.2 (1/T). After solving the equation $0.2 = \frac{\int_{h_{f,th}}^{+\infty} f(h_f)dh_f}{\int_0^{+\infty} f(h_f)dh_f}$, the $h_{f,th}$ is obtained. Further (Step 3), locating $h_{f.th}$ on a capacity threshold curve, its corresponding $v_{f.th}$ can be determined for each return period. The failure probability (Step 4) can be finally calculated through the probability density of the flood depth and velocity (Eqs. 11 and 12),

$$\begin{aligned} f(h_f, v_f) &= f(h_f; \lambda_h, k)\, f(v_f; \lambda_v, k) \\ &= \left\{ \frac{\frac{k}{\lambda_h}\left(\frac{h_f}{\lambda_h}\right)^{k-1} e^{-\left(\frac{h_f}{\lambda_h}\right)^k}}{\frac{k}{\lambda_h}\left[\left(\frac{k-1}{k}\right)^{\frac{1}{k}}\right]^{k-1} e^{-\left[\left(\frac{k-1}{k}\right)^{\frac{1}{k}}\right]^k}} \right\} \\ &\quad \left\{ \frac{\frac{k}{v_h}\left(\frac{v_f}{\lambda_v}\right)^{k-1} e^{-\left(\frac{v_f}{\lambda_v}\right)^k}}{\frac{k}{\lambda_v}\left[\left(\frac{k-1}{k}\right)^{\frac{1}{k}}\right]^{k-1} e^{-\left[\left(\frac{k-1}{k}\right)^{\frac{1}{k}}\right]^k}} \right\} \\ &\quad h_f \geqslant 0; v_f \geqslant 0. \end{aligned} \tag{11}$$

$$\begin{aligned} &P_T(v_f \geq CTC | T \geq T_d) \\ &= \frac{\int_{h_{f,th}}^{h_{f,max}} \int_{CTC}^{+\infty} f(h_f, v_f)\, dv_f dh_f}{\int_{h_{f,th}}^{h_{f,max}} \int_0^{+\infty} f(h_f, v_f)\, dv_f dh_f}, \end{aligned} \tag{12}$$

Where CTC refers to capacity threshold curve function, T_d is the design flood return period, $h_{f.th}$ refers to the corresponding threshold flood depth, $h_{f.max}$ refers to the maximum flood depth, $f(v_f,v_f)$ is the combined probability density of the flood depth and velocity as they are treated independently [14].

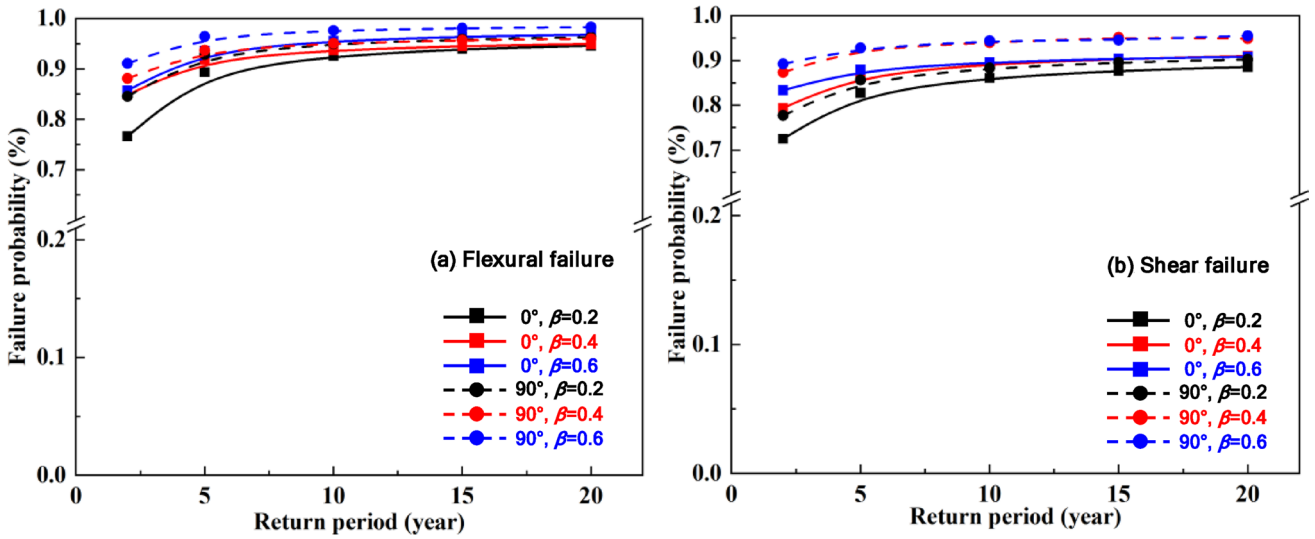

Fig. 16 Risk curves showing substation failure probability at various return periods (P_T) when $\gamma_M = 1$: **a** flexural failure; **b** shear failure

As shown in Fig. 16, the failure probability curves begin to plateau around a 10-year return period, indicating that the marginal increase in risk becomes limited beyond this point. This suggests that designing for a 10-year return period may offer a reasonable balance between risk mitigation and construction cost. While specific design recommendations will depend on local standards and acceptable risk criteria, this finding can support asset owners and policymakers in identifying cost-effective design thresholds, particularly for substations in moderate-risk regions. Overall, the risk curve can assist in planning the most appropriate interventions for substation buildings.

Conclusion

This paper presents an approach for quantifying the structural failure probabilities of a typical masonry chamber-housed substation subjected to flood events, employing a one-way CFD–Finite Element transient coupling model to assess resilience. For the particular substation building characteristics and flow regimes examined here, the key findings are as follows:

(1) The proposed one-way CFD coupling model effectively captures the complex loading from flood flows, including hydrostatic, hydrodynamic, and debris impact forces on the substation chambers. Two validations demonstrate the CFD model's ability to simulate the multifaceted nature of flood impacts to a reasonable level of accuracy.
(2) Fragility and risk curves, derived using a normalised Weibull function, further reveal that neglecting debris impact leads to an underestimation of wall forces by 60% to 83%. These findings underscore the need to revise design guidelines to incorporate debris effects and to inform appropriate retrofitting strategies for existing substations.
(3) Fragility and risk curves help assess substation chamber resilience to flooding. For floods under 0.5 m, debris size and impact angle greatly influence failure probability, with larger debris ($\beta_d > 0.4$) and a 90° impact angle being the most damaging. Mitigation may include debris traps or strengthening the masonry wall with reinforcement. At 1.5 m flood depth, failure probability nears 100%, suggesting substations should be considered failed. Risk curves further recommend designing substations to withstand 1-in-10-year flood events to enhance resilience.

In reality, the interaction between flood flows, debris and the substation chambers is complex and dependent on the specifics of the hydraulic conditions, the chamber characteristics and the location. There is a very large parameter space, and the findings in the present article are shaped by certain assumptions and limitations. For example, the analysis here focused on a single type of floating debris, whereas in reality, floodwaters often carry multiple debris objects, their combined impacts and different angles could result in more severe structural responses. Future work will incorporate varying debris shapes, intensities and concentrations to better capture the cumulative effects of debris-laden flows on the fragility of substations and electrical equipment inside, and will further develop an analytical correction factor aligned with existing global design standards as future work following a comprehensive review. Additionally, this study assumes one-way fluid–structure interaction, which is appropriate for relatively rigid structures. However, in

cases where the wall undergoes significant deflection before failure, this assumption may reduce accuracy by neglecting the feedback between fluid motion and structural response. Future work will consider implementing two-way coupling to improve result fidelity under such conditions.

Acknowledgements We gratefully acknowledge the financial support of the Global Challenges Research Fund (GCRF) for the PhD studentship. We also sincerely thank Tenaga Nasional Berhad, Malaysia, for the public data on substation design.

Data availability All data, models, or codes that support the findings of this study are available from the corresponding author upon reasonable request.

Declarations

Conflict of interest On behalf of all authors, the corresponding author states that there is no conflict of interest.

References

1. EM-DAT (2024) The international disaster database. Available at: https://public.emdat.be/data. Accessed 12 Oct 2024
2. TNB (2015) TNB recorded RM20m losses due to flood, New Straits Times, 22 September. Available at: https://www.nst.com.my/news/2015/09/tnb-recorded-rm20m-losses-due-flood. Accessed 14 Feb 2024
3. Malay Mail (2021) TNB shuts down 333 power substations in six states hit by floods, *Malay Mail*, 19 December. Available at: https://www.malaymail.com/news/malaysia/2021/12/19/tnb-shuts-down-333-power-substations-in-six-states-hit-of-floods/2029683. Accessed 10 Oct 2024
4. The Star (2023) Floods: TNB shuts down 28 substations in Johor'. The Star, 1 March. Available at: https://www.thestar.com.my/news/nation/2023/03/01/floods-tnb-shuts-down-28-substations-in-johor. Accessed 10 Oct 2024
5. SP Energy Networks (n.d.) SUB-03-025: Substation design manual. Available at: https://www.spenergynetworks.co.uk/userfiles/file/SUB-03-025.pdf. Accessed 1 Aug 2024
6. Zhang C, Ali A, Sun L, Bibi T (2021) Investigation on low-cost friction-based isolation systems for masonry building structures: experimental and numerical studies. Eng Struct 243:112645
7. Ali A, Zhang C, Bibi T, Sun L (2023) Improving the efficiency of a novel controlled-sliding-based isolation system for brick masonry structures. J Struct Eng (ASCE) 150(2):12570
8. Ali A, Zhang C, Bibi T, Sun L (2024) Experimental investigation of sliding-based isolation system with re-centering functions for seismic protection of masonry structures. Structures 60:105871
9. Si GW, Chen XQ, Chen JG, Zhao WY, Li S, Li XN (2022) Failure criteria of unreinforced masonry walls of rural buildings under the impact of flash floods in mountainous regions. J Mt Sci 19(12):3388–3406
10. Movahednia M, Kargarian A, Ozdemir CE, Hagen SC (2021) Power grid resilience enhancement via protecting electrical substations against flood hazards: a stochastic framework. IEEE Trans Ind Inform 18(3):2132–2143
11. Energy Networks Association (ENA) (2018) Resilience to flooding of grid and primary substations. Available at: https://www.ena-eng.org/ena-docs/D0C3XTRACT/ENA_ET_138_Extract_180902050400.pdf. Accessed 10 Oct 2024
12. Souto L, Yip J, Wu W-Y, Austgen B, Kutanoglu E, Hasenbein J, Yang Z-L, King C, Santoso S (2022) Power system resilience to floods: modeling, impact assessment, and mid-term mitigation strategies. Int J Electr Power Energy Syst 135:107545
13. Li W, Ceseña EAM, Cunningham LS, Panteli M, Schultz DM, Mander S, Gan CK, Mancarella P (2022) Assessing power system resilience to floods: a geo-referenced statistical model for substation inundation failures. In: 2022 IEEE PES innovative smart grid technologies conference europe (ISGT-Europe), pp 1–5. IEEE
14. Li W, Cunningham LS, Schultz DM, Mander S, Gan CK, Panteli M (2024) Structural resilience of pole-mounted substations subjected to flooding: generalised framework and a Malaysian case study. ASCE-ASME J Risk Uncertainty Eng Syst Part A Civil Eng 10(2):04024008
15. Jansen L, Korswagen PA, Bricker JD, Pasterkamp S, De Bruijn KM, Jonkman SN (2020) Experimental determination of pressure coefficients for flood loading of walls of Dutch terraced houses. Eng Struct 216:110647
16. Boroschek R, Santos JP (2020) Civil structural testing. In: Allemang R, Avitabile P (eds) Handbook of experimental structural dynamics. Springer, New York
17. FEMA (2011) Coastal construction manual: principles and practices of planning, siting, designing, constructing, and maintaining residential buildings in coastal areas. FEMA P-55, Vol. I. Federal Emergency Management Agency, Washington, D.C.
18. Elrond J (2022) Numerical simulation of fluid dynamics in complex systems using CFD. J Phys Conf Ser 2162(1):012020
19. Ahmadi SM, Balahang S, Abolfathi S (2024) Predicting the hydraulic response of critical transport infrastructures during extreme flood events. Eng Appl Artif Intell 133:108573
20. Zhang X, Wang BS (2020) Analysis of flood response to timber arch lounge bridge based on numerical simulation. Urban Roads Bridges Flood Control 5:243–248 (**in Chinese**)
21. DRD (n.d.) Ansys fluent product landing page. Available at: https://www.drd.com/product-landing-page-ansys-fluent/. Accessed 7 Jan 2025
22. Reynolds O (1895) On the dynamical theory of incompressible viscous fluids and the determination of the criterion. Philos Trans R Soc Lond A 186:123–164
23. Menter FR (1994) Two-equation eddy-viscosity turbulence models for engineering applications. AIAA J 32(8):1598–1605
24. Kestin J, Sokolov M, Wakeham WA (n.d.) Viscosity of liquid water in the range -8°C to 150°C'. Brown University, Providence, Rhode Island
25. Ducrocq T, Cassan L, Chorda J, Roux H (2017) Flow and drag force around a free surface piercing cylinder for environmental applications. Environ Fluid Mech 17(4):629–645
26. Haehnel RB, Daly SF (2004) Maximum impact force of woody debris on floodplain structures. J Hydraul Eng 130(2):112–120

27. Como A, Mahmoud H (2013) Numerical evaluation of tsunami debris impact loading on wooden structural walls. Eng Struct 56:1249–1261
28. Xiong Y, Liang Q, Zheng J, Stolle J, Nistor I, Wang G (2022) A fully coupled hydrodynamic-DEM model for simulating debris dynamics and impact forces. Ocean Eng 255:111468
29. European Committee for Standardisation (CEN) (2005). EN 1996-1-1: Eurocode 6: design of masonry structures—part 1-1: general rules for reinforced and unreinforced masonry structures. CEN, Brussels
30. Majtan E, Cunningham LS, Rogers BD (2023) Numerical study on the structural response of a masonry arch bridge subject to flood flow and debris impact. Structures 48:782–797
31. Scorzini AR, Radice A, Molinari D (2018) A new tool to estimate inundation depths by spatial interpolation (RAPIDE): design, application and impact on quantitative assessment of flood damages. Water 10(12):1805
32. Kreibich H, Piroth K, Seifert I, Maiwald H, Kunert U, Schwarz J, Merz B, Thieken AH (2009) Is flow velocity a significant parameter in flood damage modelling? Nat Hazards Earth Syst Sci 9(5):1679–1692
33. European Committee for Standardisation (CEN) (2002) EN 1991-1-1: Eurocode 1: actions on structures—Part 1–1: General Actions - Densities, Self-weight, Imposed Loads for Buildings. CEN, Brussels